Food Chemistry: X 24 (2024) 102050

Contents lists available at ScienceDirect

Food Chemistry: X

journal homepage: www.sciencedirect.com/journal/food-chemistry-x

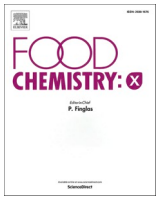

# Improving stability and bioavailability of ACNs based on Gellan gum-whey protein isolate nanocomplexes

Xin Zhou [a,b], Na Guo [a], Fangyan Zhang [a], Kaili Zhuo [a], Guilan Zhu [a,*,1]

[a] School of Biology and Food Engineering, Anhui Province Green Food Collaborative Technology Service Center for Rural Revitalization, Hefei Normal University, Hefei 230601, Anhui Province, PR China
[b] School of Life Sciences, Anhui University, Hefei, 230601, Anhui, China

ARTICLE INFO

*Keywords:*
Blueberry anthocyanins
Gellan gum
Whey protein isolate
Antioxidant activity
Stability

ABSTRACT

Blueberry anthocyanins (ACNs) have been widely applied in the food industry and medicine due to their numerous beneficial properties. However, the stability of ACNs is extremely poor. This study aimed to develop a delivery system for ACNs using nanocomplexes prepared from gellan gum (GG) and whey protein isolate (WPI) via Maillard reaction. The effects of the GG-WPI nanocomplexes on the stability, antioxidant capacity, and bioavailability of ACNs were investigated. FTIR, fluorescence spectroscopy, and UV–vis absorption spectroscopy revealed covalent bonding between the GG and WPI in the nanocomplexes. The nanocomplex demonstrated a good loading efficiency for ACNs (60.34 %), with a particle size of 368.42 nm. It also showed better stability and bioaccessibility than free ACNs, and their DPPH radical scavenging capacity reached a maximum of 63.11 %. Our research is significant for developing novel multifunctional foods and constructing high-performance food delivery systems.

## 1. Introduction

Blueberry anthocyanins (ACNs) are natural water-soluble plant pigments belonging to the class of flavonoid polyphenol compounds (Li et al., 2019). They include malvidin, delphinidin, cyanidin, peonidin, and petunidin (Veberic et al., 2015). ACNs have excellent antioxidant activity, anti-inflammatory activity, prevent cardiovascular diseases, alleviate obesity, and so on. The functions of ACNs enable their widespread application in the food industry, medicine, and other fields (Chen et al., 2023). However, ACNs are notoriously unstable in processing and storage, and they are vulnerable to environmental stresses, such as light, pH, temperature and ascorbic acid (Belwal et al., 2019; Duan et al., 2024). This leads to a decline in their functional properties. Although ACNs are relatively stable in the gastric environment, they tend to decompose and be transformed in the alkaline environment of intestine. It leads to a decrease in their bioavailability (Correa-Betanzo et al., 2014). Therefore, a series of physical and chemical methods have been developed to enhance the stability and bioavailability of ACNs (Cheng et al., 2023). Physical methods include copigmentation and interaction with macromolecules such as polysaccharides and proteins. Chemical methods include encapsulation (Liu et al., 2023), acylation, glycosylation (Wang et al., 2018), and methoxylation (Liu et al., 2022). The carriers commonly used in physical and chemical methods above are generally polysaccharides and proteins. Polysaccharides commonly used include chitosan (Xue et al., 2022), chitosan derivatives (Liu et al., 2023), and sodium alginate (Li et al., 2023). Proteins include bovine serum albumin (Zang et al., 2022), whey protein isolate (Zang et al., 2021), and ferritin (Huang et al., 2023). The affinity of copolymer structures produced by physical methods is unknown and highly dependent on environmental conditions (Fu et al., 2021). Compared with the physical method, the chemical method can improve the stability of ACNs better and have a slow-release effect. Increasing research indicates that encapsulation is an excellent method for delivering ACNs (Ge et al., 2018). However, encapsulation with a single wall material is easily affected by environmental factors. Compared with ACNs-loaded single-wall material, ACNs-loaded polysaccharide-protein complex displayed better-sustained ACNs release, stability, and bioavailability (Cao et al., 2024), such as the complex with ovalbumin and sulfated-polysaccharides (Dong et al., 2024), and the complex with chitosan derivatives and β-Lactoglobulin (Ge et al., 2019).

Gellan gum (GG) is an anionic extracellular polysaccharide produced by fermenting *Sphingomonas paucimobilis*, which is water-soluble and

* Corresponding author.
*E-mail address:* zhuguilan13@126.com (G. Zhu).
[1] The author jointly supervised this work: Guilan Zhu

https://doi.org/10.1016/j.fochx.2024.102050
Received 28 October 2024; Received in revised form 18 November 2024; Accepted 27 November 2024
Available online 29 November 2024

easy to form gel at low temperatures. It has an anionic character (pKa of 3.5) due to the presence of glucuronic acid on its structure, and has outstanding potential with food function factors (Duarte et al., 2022). It was found that gellan gum could improve the thermal stability of purple sweet potato anthocyanins in the presence of ascorbic acid (Xu et al., 2019). Nevertheless, it is still unknown whether gellan gum can mitigate the effects of other environmental factors on anthocyanins.

Whey protein isolate (WPI) is a high-purity whey protein obtained from whey protein through specific methods, such as physical heating, ion exchange, etc. Due to its good gelling, emulsification, foaming and ligand binding ability, it is often regarded as a biological material with excellent properties. In addition to being added to food as functional substances and nutrients, it is also increasingly used as a carrier material in food delivery systems (Chen et al., 2021). WPI has demonstrated a beneficial impact on the stability and antioxidant capacity of ACNs. However, proteins are more sensitive to environmental conditions and generally have poor functional properties near their isoelectric points or at higher temperatures. The preparation of protein-polysaccharide covalent complexes based on the Maillard reaction is often used to improve protein properties (He et al., 2021). To date, the potential of GG-WPI nanocomplexes to improve the stability and bioavailability of ACNs has not been studied. The study is based on the hypothesis that (1) gellan gum and whey protein isolate can form nanocomplexes loaded with blueberry anthocyanins and (2) gellan gum-whey protein isolate nanocomplexes can improve the stability of blueberry anthocyanins.

In this study, a binary nanocomplex using high acyl GG and WPI was prepared to encapsulate ACNs. The effects of these nanocomplexes on ACN stability, antioxidant activity, gastrointestinal release, and bioavailability were investigated.

## 2. Materials and methods

### 2.1. Materials

High acyl gellan gum was food-grade and purchased from Hefei Bomei Biotechnology Co., Ltd. The acyl content of high acyl gellan gum is 11.67 %, and the purity is 99.5 %. Whey protein isolate (purity is 93 %) was obtained from Hilmar Ingredients (Hilmar, CA, USA). Blueberry anthocyanins (purity is 25 %) was purchased from Ningshan Guosheng Biological Technology Co., Ltd.

### 2.2. Preparation of GG-WPI covalent nanocomplexes

The GG-WPI covalent complexes were synthesized by referring to previous methods (Chen et al., 2019). Mixture solution of GG (0.2 *w/v* %) and WPI (0.4 w/v %) was magnetically stirred at 30 °C overnight. Then, adjusted to the pH 11.0, ultrasound equipment treated the solution for 60 min (420 W, 50 °C). After that, the solution was dialyzed against distilled water for 2 days. Finally, the solution was lyophilized to get the GG-WPI nanocomplexes.

### 2.3. Preparation of ACNs-loaded GG-WPI nanocomplexes

The complex solutions were mixed with different concentrations of ACNs solution with a volume ratio of 1:1. The mixture was stirred overnight to obtain ACNs-loaded GG-WPI complexes solutions with ACNs concentrations of 0.2 %, 0.4 %, and 0.6 %. Finally, the solution was lyophilized to get the nanocomplexes loaded with ACNs. The nanocomplexes loaded with ACNs at different concentrations were recorded as GWC-A-2, GWC-A-4, and GWC-A-6.

### 2.4. Load efficiency of ACNs

The Load efficiency of ACNs in the nanocomplexes was measured according to Dey's method with slight modification (Dey et al., 2020). The sample (0.01 g) was accurately weighed and dissolved in 10 mL of acidified ethanol solution. The mixture was stirred until fully dissolved. 1 mL of the sample solution was diluted to 10 mL with acidified ethanol, and measure the absorbance value. The following equation was used to determine Load efficiency (%) of ACNs,

$$\text{Load efficiency}(\%) = \frac{\text{Actual content}}{\text{Theoretical content}} \times 100\% \quad (1)$$

### 2.5. Particle size, polydispersity index (PDI) and zeta potential of the nanocomplexes

The nanocomplexes' particle size, polydispersity index and zeta potential were measured using a particle size and zeta potential analyzer (Brookhaven, 90Plus PALS). All measurements were carried at 25 °C, with 3 measurements per sample. Before analysis, the sample solutions were diluted with deionized water to avert multiple scattering influences.

### 2.6. Fourier transform infrared spectrum analysis

The structures of the substances were analysed using Fourier transform infrared spectroscopy. The sample was pressed into flakes, and the KPS-5 ATR probe was used for detection. All the samples were scanned from 500 to 4000 $cm^{-1}$ with a resolution of 4 $cm^{-1}$.

### 2.7. UV–vis spectroscopy measurement

An aqueous solution of equal concentrations of GG, WPI, ACNs, GG-WPI and GWC-A-6 nanocomplexes was prepared, and the UV–Vis spectra were recorded in the range of 200–800 nm.

### 2.8. Fluorescence spectrum analysis

The fluorescence spectra of WPI, GG-WPI, and GWC-A-6 nanocomplexes were determined by fluorescence spectrophotometer. Dilute the WPI, GG-WPI, and GWC-A-6 nanocomplexes to 1 mg/mL in an aqueous solution. The emission spectra were recorded in the wavelength range of 300–450 nm (emission slit width of 5 nm) under excitation at 280 nm (excitation slit width of 5 nm).

### 2.9. Thermal characteristic analysis

A synchronous thermal analyzer (TG) was used to determine the weight loss temperature of each substance in the sample. Approximately 6 mg of the sample was placed in an alumina crucible at 35 °C ~ 500 °C and 5 °C /min. The operation is carried out in 100 mL/min flowing nitrogen to prevent the sample from coming into contact with the air reacting, and affecting the substance structure. Record data and draw TGA and DTG curves.

### 2.10. SEM analysis

The samples were lyophilized by liquid nitrogen, and the natural lyophilized sections were taken and placed under a scanning electron microscope (Hitachi High-tech Co., LTD.) after gold plating, and the microstructure of the samples was observed at 500 maginification.

### 2.11. DPPH radical scavenging activity assay

The ability of ACNs to scavenge the DPPH radicals was determined based on research (Fan et al., 2018) with some modifications. The 1 mL of sample solution (1 mg/mL,dissolved in deionized water) was added to 2 mL of DPPH solution ($1.75 \times 10^{-4}$ mol/L, dissolved in anhydrous ethanol), then placed for 1 h under dark. Then, the absorbance of samples was measured at 517 nm, and anhydrous ethanol: water was 1:1 (v:v) as a reference. The free radical clearance rate was calculated by

substituting the formula (2).

$$\text{DPPH radical scavenging activity}(\%) = \left(1 - \frac{A_1 - A_2}{A_0}\right) \times 100\% \quad (2)$$

Where $A_0$ is the absorbance of the DPPH ethanol solution, $A_1$ is the absorbance of the reaction solution after 60 min, and $A_2$ is the absorbance of the sample complex ethanol solution.

### 2.12. Storage stability analysis

The stability analysis was according to (Fu et al., 2022) with some modifications. Nanocomplexes loaded with different concentrations of ACNs were prepared in solution, and free ACNs were used as control. These solutions were also put in brownglass bottles and stored at 4 °C for 10 days, and the absorbance at A520 nm was measured every two days. The retention rate of ACNs was calculated by substituting formula (3).

$$\text{Retention rate of ACNs}\ (\%) = \frac{A_i}{A_j} \times 100\% \quad (3)$$

where $A_i$ is the absorbance of ACNs after preservation, $A_j$ is the absorbance of ACNs in the original solution.

### 2.13. Bioaccessibility analysis

By simulating the digestive conditions of the gastrointestinal tract in vitro, the effect of the GG-WPI nanocomplexes on the bioavailability of ACNs was studied. Simulated gastric fluid (SGF) and intestinal fluid (SIF) were prepared according to Mao's method (Mao & McClements, 2012). The content of ACNs was determined using the method described in section 2.4. The bioavailability (BA, %) was calculated according to formula (4).

$$\text{BA}(\%) = \frac{C_t}{C_0} \times 100\% \quad (4)$$

where $C_t$ and $C_0$ represent the concentrations of ACNs in the supernatant and original solution, respectively.

### 2.14. Statistical analysis

All the experiments were performed at least in triplicate and all data were shown in terms of mean ± standard deviations. SPSS 19.0 software was used for statistical analysis. The significance of data was conducted using a one-way analysis of variance (ANOVA) and Duncan's test with $p$-value <0.05.

## 3. Results and discussion

### 3.1. Particle size, polydispersity index (PDI) and zeta potential of the nanocomplexes

As shown in Table 1, the particle sizes of all samples were between 300 nm and 400 nm. Nanocomplexes particles within this range are small and readily taken up by intestinal cells. The particle size of GWC-A-2 was smaller than GG-WPI because there were strong interactions among GG, WPI, and ACNs, resulting in a relatively compact structure (Dai et al., 2018). The particle size of GWC-A continued to grow with the increase of ACNs concentration. This result could be explained by the decreased electrostatic repulsion between nanoparticles (Dai et al., 2018). This is consistent with previous studies using chitosan (CS) and sodium alginate (ALG) to encapsulate ACNs (Chen et al., 2024).

At the same time, the PDI of all nanocomplexes was less than 0.30, which indicated good dispersion of nanocomplexes (Hua et al., 2021). The Zeta potential of the nanocomplexes was close to 30 mV, indicated ACNs nanoparticles had good physical stability (Fu et al., 2022).

The loading efficiency rose with the initial addition of ACNs. This occurred because higher ACNs content leads to more interactions and provides more opportunities for electrostatic interactions, provided the GG-WPI nanocomplexes were sufficient. The finding was consistent with the particle size results. However, when the ACNs concentration was further increased, the limited GG-WPI nanocomplexes may cause ACNs to remain free, reducing the loading efficiency (Mu et al., 2019).

**Table 1**
particle size, polydispersity index (PDI), zeta potential, and the load efficiency of GG-WPI and GWC-A

| Sample | Particle size (nm) | Polydispersity | Zeta Potential (mV) | Load efficiency (%) |
|---|---|---|---|---|
| GG-WPI | 331.21 ± 22.66$^{b}$ | 0.287 ± 0.02$^{a}$ | 27.59 ± 0.76$^{c}$ | - |
| GWC-A-2 | 306.16 ± 7.09$^{c}$ | 0.263 ± 0.02$^{a}$ | 29.33 ± 0.95$^{b}$ | 34.71 ± 0.12$^{c}$ |
| GWC-A-4 | 339.16 ± 10.03$^{b}$ | 0.293 ± 0.07$^{a}$ | 30.49 ± 1.04$^{a}$ | 54.12 ± 0.35$^{b}$ |
| GWC-A-6 | 368.42 ± 15.25$^{a}$ | 0.273 ± 0.04$^{a}$ | 29.99 ± 0.46$^{a}$ | 60.34 ± 0.17$^{a}$ |

GG, gellan gum; WPI, whey protein isolate; GWC-A, the GG-WPI nanocomplexes loaded with ACNs at different concentrations. Different letters in the same column indicate significant differences between means (p-value <0.05).

### 3.2. Fourier transform infrared spectrum analysis

The FTIR spectra of GG, WPI, GG-WPI and GWC-A nanocomplexes was represented in Fig. 1. The FTIR of GG showed the peak at 3500 $cm^{-1}$–3200 $cm^{-1}$ was due to the stretching vibration of the OH group. The characteristic bands at 1606 $cm^{-1}$ and 1406 $cm^{-1}$ were due to the asymmetric and symmetrical stretching vibration of COO- (Wu et al., 2022). The stretching vibrations of $CH_2$ and hydroxyl C—O were observed at 2932 $cm^{-1}$ and 1023 $cm^{-1}$ (Chen et al., 2019). Other authors observed similar spectra of GG (Dey et al., 2020). In the WPI spectrum, bands of amide-type I and amide-type II were observed at 1639 $cm^{-1}$ and 1514 $cm^{-1}$, characteristic bands of proteins (Falsafi et al., 2022; Jia et al., 2020). Characteristic peaks near 1430 $cm^{-1}$ were attributed to acylamino-III or C-$NH_2$ stretching vibrations. It was observed that the OH group stretching vibration of GG-WPI was shifted from 3348 $cm^{-1}$ to 3278 $cm^{-1}$ and significantly enhanced, compared with GG. The number of OH groups increased due to the introduction of WPI, enlarged the corresponding absorption peak intensity (Chen et al.,2021). The absorption peak at 1637 $cm^{-1}$ was caused by the C═O stretching vibration in the peptide bond due to the presence of peptide bonds in WPI. In addition, the absorption peaks of GG-WPI disappeared at 1751 $cm^{-1}$,1571 $cm^{-1}$, 1514 $cm^{-1}$, and 1359 $cm^{-1}$, and the absorption peaks were enhanced at 1046 $cm^{-1}$, indicated that newly formed C—N covalent bonds were generated in the GG-WPI nanocomplexes. This is consistent with previous studies between rapeseed protein isolate and glucan (Zhu et al., 2008) and between WPI and glucan (Mundlia et al., 2021). The enhancement of the peak of GWC-A at 1640–1630 $cm^{-1}$ is caused by the vibration contraction of the benzene ring C═C in ACNs (Bao et al., 2024).

### 3.3. UV–vis spectroscopy analysis

As shown in Fig. 2, the maximum absorption peak of GG was at 256 nm, and that of WPI was at 280 nm (Chen et al., 2021). However, the maximum absorption peak of the GG-WPI nanocomplexes was at 277 nm, which was blue-shifted compared to WPI, because GG and WPI formed a covalent bound (Tao et al., 2022). The maximum absorption peak of GWC-A was red-shifted compared with ACNs, due to the enhanced hydrogen bond interaction after the loading of ACNs on the GG-WPI nanocomplexes.

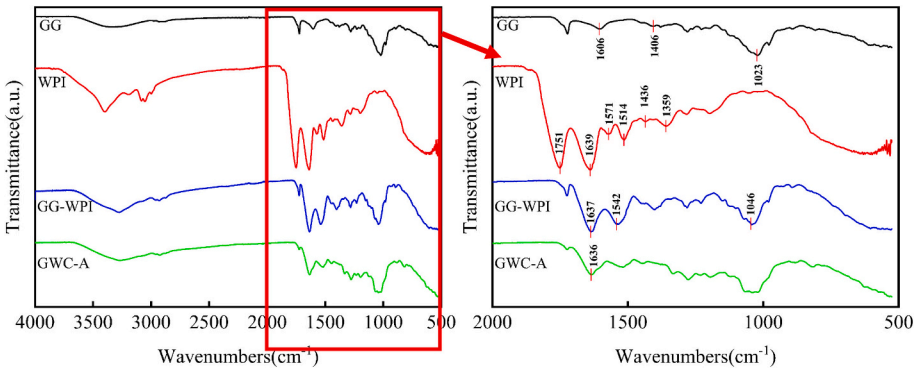


**Fig. 1.** Fourier transform infrared spectra of GG, WPI, GG-WPI, and GWC-A.

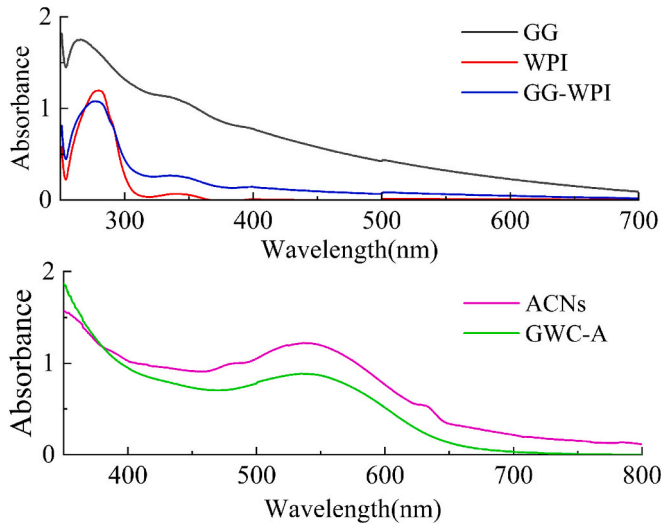


**Fig. 2.** UV–vis spectrum of GG, WPI, GG-WPI, ACNs and GWC-A.

### 3.4. Fluorescence spectrum analysis

The fluorescence spectra were shown in Fig. 3. At an excitation wavelength of 280 nm, WPI showed maximum emission intensity ($\lambda_{max}$) at 332 nm. For the GG-WPI nanocomplexes, a decrease in fluorescence intensity and a red-shift in λmax (340 nm) were observed. It has been reported that polysaccharide-protein complexes obtained by ultrasonic treatment exhibit lower fluorescence intensity compared to native proteins. This phenomenon was attributed to the shielding effect of polysaccharide chains bound to protein (He et al., 2021). Studies have shown significant red-shifts in the maximum absorption peak of Try (Tryptophan) fluorescence, indicated that covalent binding causes the change of the protein's tertiary structure. This change suggested that Try moved to a more hydrophilic environment, directly related to the hydrophilic hydroxyl and carboxyl groups introduced by gellan gum. It was observed that the λmax of GWC-A was red-shifted from 340 nm to 368 nm, and the fluorescence intensity decreased, indicated that ACNs quench the protein fluorescence (Ma et al., 2024).

### 3.5. Thermal characteristic analysis

Fig. 4 showed the TGA curves of GG, WPI, GG-WPI nanocomplexes, and GWC-A. The mass of the substance decreased slightly at 50 °C ~ 200 °C, which may be caused by the loss of free and bound water on the materials (Diao et al., 2020). Since the sample was freeze-dried, the water content was low, and the weight loss was not obvious. At 200 °C ~ 400 °C, the mass of the material linearly reduced, which was mainly due to the degradation and decomposition of the material. The findings were in accordance with the thermal degradation of lycopene embedded in a whey protein isolate-xylo-oligosaccharide conjugate prepared by the Maillard reaction (Jia et al., 2020). The DTG curve showed a sharp exothermic peak of GG was approximately 240 °C (Dey et al., 2020), and that of WPI was around 295 °C. The lower final weight loss rate for WPI was due to the presence of inorganic salts in the WPI power (Falsafi et al., 2022). Compared with GG, the weight loss peak of GG-WPI

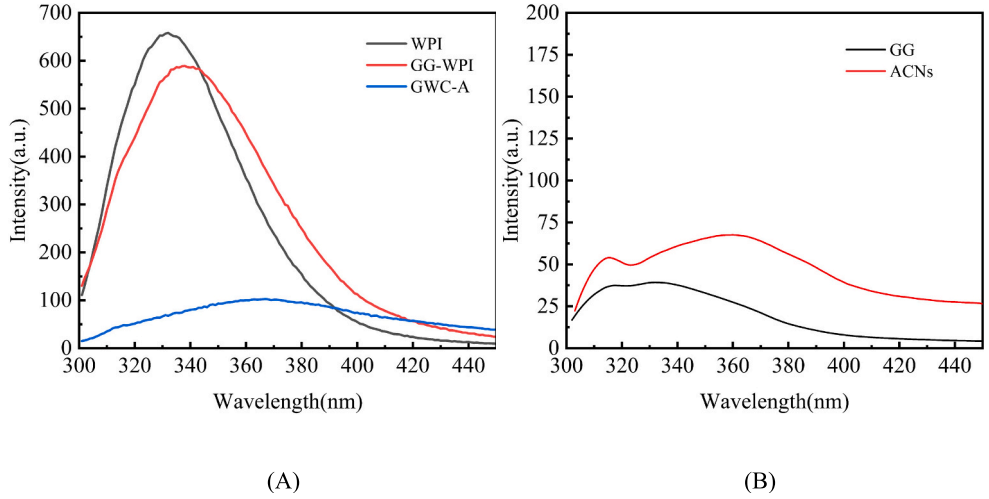


**Fig. 3.** Fluorescence spectrum of WPI, GG-WPI, GWC-A (A), and GG, ACNs (B).

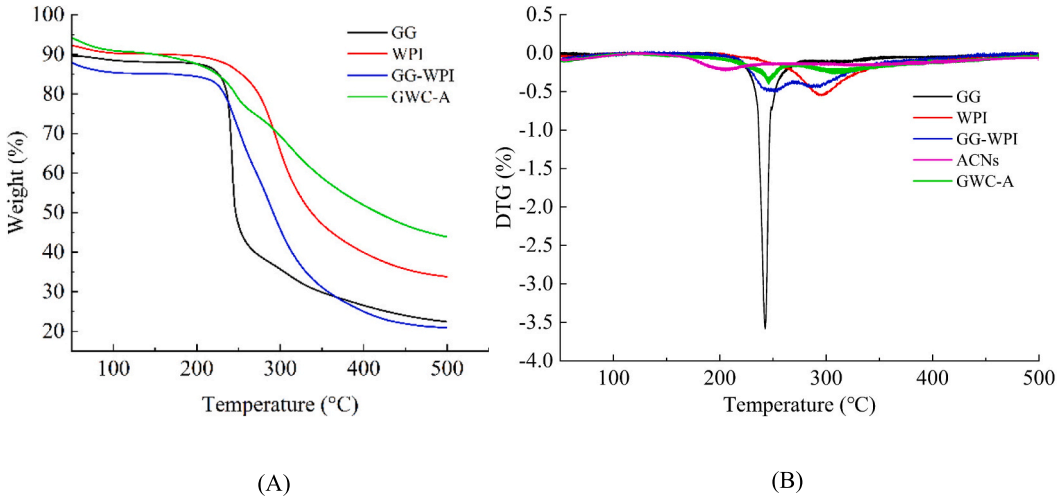


**Fig. 4.** TGA thermograms of GG, WPI, GG-WPI, GWC-A (A), and DTG thermograms of GG, WPI, GG-WPI, ACNs and GWC-A (B).

increased from 240 °C to 250 °C, and the weight loss rate was decreased. This indicated that the interaction between GG and WPI enhanced the thermal stability of the covalence complexes and improved its heat resistance, which was beneficial for its use as a delivery system wall material (Wu et al., 2022). The weight loss temperature of ACNs was 204 °C, while the weight loss temperature of GWC-A was 245 °C, indicated that the thermal stability of ACNs could be improved by loading ACNs with GG-WPI nanocomplexes (Liu et al., 2023), thereby enhancing the stability of ACNs during storage and processing.

### 3.6. SEM analysis

The SEM of GG-WPI and GWC-A nanocomplexes with a magnification of 500× shown in Fig. 5. As a result, the GG-WPI covalent complexes had a relatively obvious cavity structure with compact and ordered folded lamella (Mundlia et al., 2021). After loading ACNs, the SEM images showed the cavity structure shrank and the irregular bulk structure increased, indicated that ACNs and GG-WPI covalent complexes were cross-linked through hydrogen bonds. These changes in the complexes confirmed the successful encapsulation of ACNs within the GG-WPI nanocomplexes (Liu et al., 2023).

### 3.7. Antioxidant activity, storage stability and bioaccessibility analysis

The radical scavenging activity of ACNs and GWC-A was shown in Fig. 6A. The DPPH radical scavenging activity of all GWC-A samples was significantly enhanced in comparison to free ACNs. This was because free ACNs were highly susceptible to degradation from external factors such as light and temperature. Encapsulated ACNs within the GG-WPI nanocomplexes minimized their contact, prevented decomposition and preserved their antioxidant capacity (Bao et al., 2024). Additionally, as the loading rate of ACNs increases, the antioxidant activity also gradually improved.

Fig. 6B shown the retention rate of free ACNs and ACNs in nanocomplexes after 10 days of storage at 4 °C in the dark. The retention rate of free ACNs declined almost linearly over time, dropped to just 30.36 % on day 10. In contrast, the retention rates of ACNs in nanocomplexes with different loading rates decreased more slowly and remained higher than those of free ACNs. On day 10, the retention rates of ACNs in GWC-A-2, GWC-A-4, and GWC-A-6 were 57.26 %, 60.69 %, and 72.12 %,

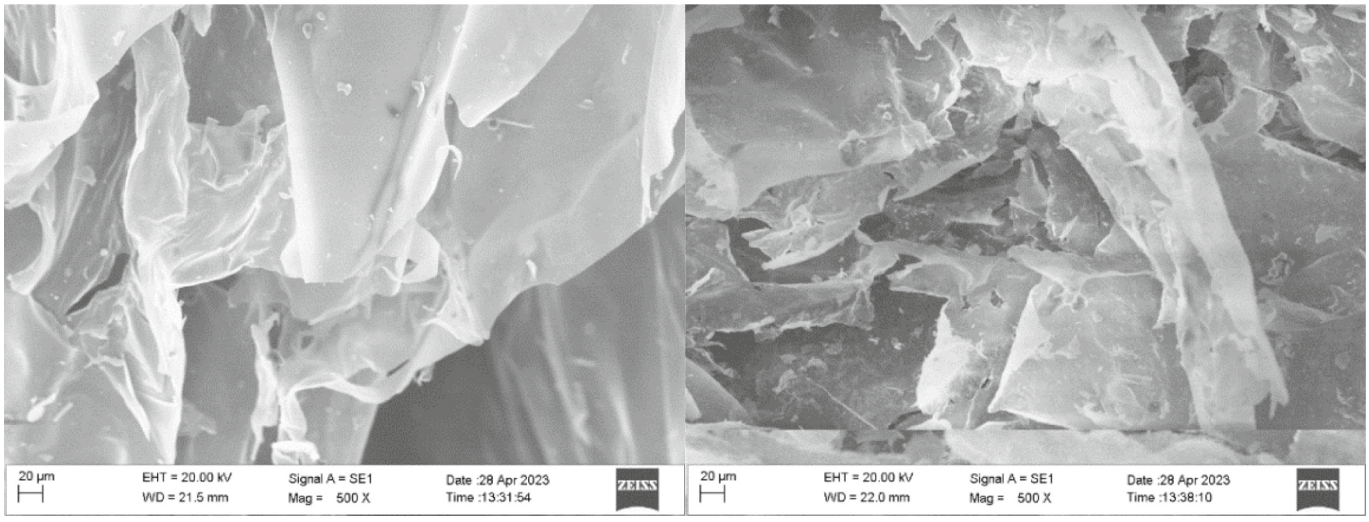


**Fig. 5.** Scanning electron micrographs of (A) GG-WPI and (B) GWC-A at 500×, respectively.

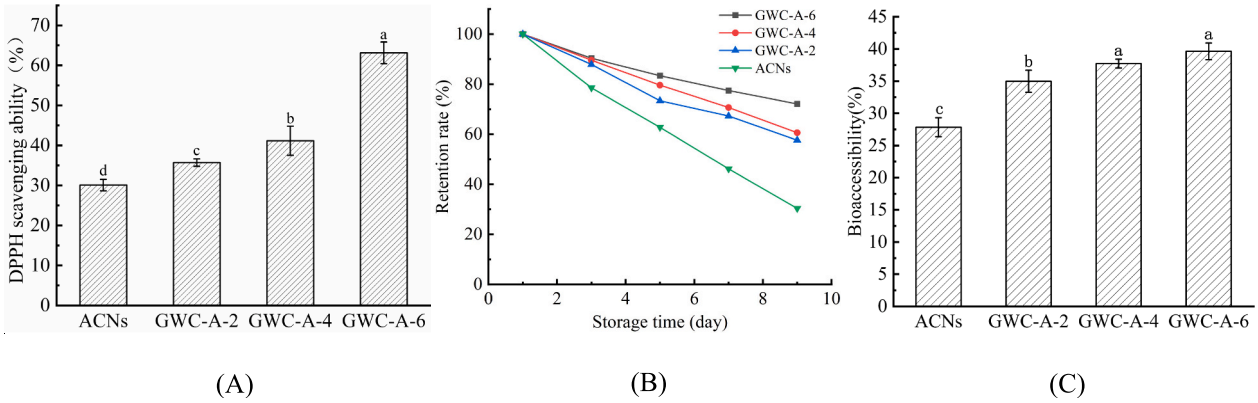


**Fig. 6.** DPPH scavenging ability(A), storage stability(B) and bioaccessibility of ACNs and GWC-A. Different lowercase letters indicate significant differences between groups ($p < 0.05$).

respectively. This indicated that as the loading rate of ACNs increased, the retention rate also improved. On the 3 day, the GG-WPI nanocomplexes showed a stronger protective effect on ACNs. These results confirmed that GG-WPI nanocomplexes effectively encapsulated ACNs, and reduced the impact of environmental factors on ACNs stability, which is consistent with previous studies (Mansour et al., 2020).

As shown in Fig. 6C, the bioaccessibility of free ACNs is only 28.29 %, indiacated that most ACNs degrade during gastrointestinal digestion. In contrast, the bioaccessibility of ACNs, within the GG-WPI nanocomplexes was significantly higher ($p < 0.05$) than that of free ACNs, due to the nanocomplexes slowing the release rate of ACNs during digestion. The nanocomplexes loaded with different concentrations of ACNs did not show significant differences in their sustained release, which may be due to the relatively low initial concentration of ACNs. However, compared to free ACNs, the GG-WPI nanocomplexes still demonstrated better protective effects. These results suggested that the GG-WPI nanocomplexes delivery system may slow or prevent degradation and increase ACNs bioaccessibility (Fan et al., 2018). This finding is consistent with the Wang et al. (2021), they noted that anthocyanins in chitosan hydrochloride/carboxymethyl chitosan and whey protein isolate nanocomplexes were more stable and released more slowly during simulated gastrointestinal digestion.

## 4. Conclusion

In this study, GG-WPI nanocomplexes were prepared using an Maillard reaction. Structural characterization confirmed the formation of covalent bonds between GG and WPI. Based on these covalent complexes, nanocomplexes loaded with ACNs were developed and analysed for thermal stability, particle size, and loading efficiency. The results showed that the thermal stability of ACNs was signigicantly improved. At an ACNs concentration of 6 mg/mL, the nanocomplex size was 368.42 ± 15.25 nm with a loading rate of 60.34 %. Antioxidant activity, stability, and bioavailability analysis revealed that the functional properties of ACNs in nanocomplexes were superior to those of free ACNs. The DPPH radical scavenging ability of the GWC-A-6 reached 63.11 %, nearly double that of free ACNs. During a Bioaccessibility analysis, the nanocomplexes provided significant protection for ACNs, reduced their degradation rate during gastrointestinal digestion, and improved bioavailability. Nevertheless, more in vivo animal and human studies needed to determine whether encapsulating ACNs in nanocomplexes also improves its in vivo bioavailability and bioactivity. This study provides a promising carrier for the further application of bioactive substances with poor stability and low utilization in food processing.

## CRediT authorship contribution statement

**Xin Zhou:** Writing – original draft, Validation, Methodology, Investigation. **Na Guo:** Investigation, Formal analysis. **Fangyan Zhang:** Methodology, Formal analysis, Conceptualization. **Kaili Zhuo:** Validation, Project administration, Methodology, Investigation. **Guilan Zhu:** Writing – review & editing, Supervision, Data curation, Conceptualization.

## Declaration of competing interest

The authors declare that they have no conflicts of interest.

## Acknowledgements

This work was supported by the Natural Science Foundation of the Higher Education Institutions of Anhui Province (2022AH040288 & 2022AH052147) and Anhui Province Green Food Collaborative Technology Service Center for Rural Revitalization (GXXT-2023-041 & GXXT-2022-078).

## Data availability

The data that has been used is confidential.

## References

Bao, Y., Wang, M., Si, X., Li, D., Gui, H., Jiang, Q., … Li, B. (2024). Customized development of 3D printed anthocyanin-phycocyanin polychromatic oral film via chondroitin sulfate homeostasis: A platform based on starch and κ-carrageenan. *Carbohydrate Polymers, 330*, Article 121817.

Belwal, T., Huang, H., Li, L., Duan, Z., Zhang, X., Aalim, H., & Luo, Z. (2019). Optimization model for ultrasonic-assisted and scale-up extraction of anthocyanins from Pyrus communis 'Starkrimson' fruit peel. *Food Chemistry, 297*, Article 124993.

Cao, Y., Gou, Q., Song, Z., Zhang, L., Yu, Q., Zhu, X., & Li, S. (2024). Smart carrageenan/carboxymethyl cellulose films combined with zein/gellan gum microcapsules encapsulated by composite anthocyanins for chilled beef freshness monitoring. *Food Hydrocolloids, 153*, Article 110059.

Chen, B., Ai, C., He, Y., Zheng, Y., Chen, L., & Teng, H. (2024). Preparation and structural characterization of chitosan-sodium alginate nanocapsules and their effects on the stability and antioxidant activity of blueberry anthocyanins. *Food Chemistry: X, 23*, Article 101744.

Chen, W., Ma, X., Wang, W., Lv, R., Guo, M., Ding, T., … Liu, D. (2019). Preparation of modified whey protein isolate with gum acacia by ultrasound maillard reaction. *Food Hydrocolloids, 95*, 298–307.

Chen, Y., Belwal, T., Xu, Y., Ma, Q., Li, D., Li, L., Xiao, H., & Luo, Z. (2023). Updated insights into anthocyanin stability behavior from bases to cases: Why and why not anthocyanins lose during food processing. *Critical Reviews in Food Science and Nutrition, 63*(27), 8639–8671.

Chen, Y., Huang, F., Xie, B., Sun, Z., McClements, D. J., & Deng, Q. (2021). Fabrication and characterization of whey protein isolates-lotus seedpod proanthocyanin conplex: Its potential application in oxidizable emulsions. *Food Chemistry, 346*, Article 128680.

Cheng, Y., Liu, J., Li, L., Ren, J., Lu, J., & Luo, F. (2023). Advances in embedding techniques of anthocyanins: Improving stability, bioactivity and bioavailability. *Food Chemistry, X*, Article 100983.
Correa-Betanzo, J., Allen-Vercoe, E., McDonald, J., Schroeter, K., Corredig, M., & Paliyath, G. (2014). Stability and biological activity of wild blueberry (Vaccinium angustifolium) polyphenols during simulated in vitro gastrointestinal digestion. *Food Chemistry, 165*, 522–531.
Dai, L., Li, R., Wei, Y., Sun, C., Mao, L., & Gao, Y. (2018). Fabrication of zein and rhamnolipid complex nanoparticles to enhance the stability and in vitro release of curcumin. *Food Hydrocolloids, 77*, 617–628.
Dey, M., Ghosh, B., & Giri, T. K. (2020). Enhanced intestinal stability and pH sensitive release of quercetin in GIT through gellan gum hydrogels. *Colloids and Surfaces B: Biointerfaces, 196*, Article 111341.
Diao, Y., Yu, X., Zhang, C., & Jing, Y. (2020). Quercetin-grafted chitosan prepared by free radical grafting: Characterization and evaluation of antioxidant and antibacterial properties. *Journal of Food Science and Technology, 57*, 2259–2268.
Dong, R., Huang, Z., Ma, W., Yu, Q., Xie, J., Tian, J., … Chen, Y. (2024). Fabrication of nanocomplexes for anthocyanins delivery by ovalbumin and differently dense sulphate half-ester polysaccharides nanocarriers: Enhanced stability, bio-accessibility, and antioxidant properties. *Food Chemistry, 432*, Article 137263.
Duan, C., Xiao, X., Yu, Y., Xu, M., Zhang, Y., Liu, X., … Wang, J. (2024). In situ Raman characterization of the stability of blueberry anthocyanins in aqueous solutions under perturbations in temperature, UV, pH. *Food Chemistry, 431*, Article 137155.
Duarte, L. G., Alencar, W. M., Iacuzio, R., Silva, N. C., & Picone, C. S. (2022). Synthesis, characterization and application of antibacterial lactoferrin nanoparticles. *Current Research in Food Science, 5*, 642–652.
Falsafi, S. R., Rostamabadi, H., Nishinari, K., Amani, R., & Jafari, S. M. (2022). The role of emulsification strategy on the electrospinning of β-carotene-loaded emulsions stabilized by gum Arabic and whey protein isolate. *Food Chemistry, 374*, Article 131826.
Fan, Y., Liu, Y., Gao, L., Zhang, Y., & Yi, J. (2018). Improved chemical stability and cellular antioxidant activity of resveratrol in zein nanoparticle with bovine serum albumin-caffeic acid conjugate. *Food Chemistry, 261*, 283–291.
Fu, J. J., Sun, C., Tan, Z. F., Zhang, G. Y., Chen, G. B., & Song, L. (2022). Nanocomplexes of curcumin and glycated bovine serum albumin: The formation mechanism and effect of glycation on their physicochemical properties. *Food Chemistry, 368*, Article 130651.
Fu, X., Wang, D., Belwal, T., Xie, J., Xu, Y., Li, L., Zou, L., Zhang, L., & Luo, Z. (2021). Natural deep eutectic solvent enhanced pulse-ultrasonication assisted extraction as a multi-stability protective and efficient green strategy to extract anthocyanin from blueberry pomace. *Lwt, 144*, Article 111220.
Ge, J., Yue, P., Chi, J., Liang, J., & Gao, X. (2018). Formation and stability of anthocyanins-loaded nanocomplexes prepared with chitosan hydrochloride and carboxymethyl chitosan. *Food Hydrocolloids, 74*, 23–31.
Ge, J., Yue, X., Wang, S., Chi, J., Liang, J., Sun, Y., … Yue, P. (2019). Nanocomplexes composed of chitosan derivatives and β-Lactoglobulin as a carrier for anthocyanins: Preparation, stability and bioavailability in vitro. *Food Research International, 116*, 336–345.
He, W., Tian, L., Zhang, S., & Pan, S. (2021). A novel method to prepare protein-polysaccharide conjugates with high grafting and low browning: Application in encapsulating curcumin. *Lwt, 145*, Article 111349.
Hua, C., Yu, W., Yang, M., Cai, Q., Gao, T., Zhang, S., … Liu, Y. (2021). Casein-pectin nanocomplexes as a potential oral delivery system for improving stability and bioactivity of curcumin. *Colloid and Polymer Science, 299*, 1557–1566.
Huang, W., Zhao, X., Chai, Z., Herrera-Balandrano, D. D., Li, B., Yang, Y., … Tu, Z. (2023). Improving blueberry Anthocyanins' stability using a ferritin Nanocarrier. *Molecules, 28*(15), 5844.
Jia, C., Cao, D., Ji, S., Lin, W., Zhang, X., & Muhoza, B. (2020). Whey protein isolate conjugated with xylo-oligosaccharides via maillard reaction: Characterization, antioxidant capacity, and application for lycopene microencapsulation. *Lwt, 118*, Article 108837.
Li, D., Zhang, X., Li, L., Aghdam, M. S., Wei, X., Liu, J., Xu, Y., & Luo, Z. (2019). Elevated CO2 delayed the chlorophyll degradation and anthocyanin accumulation in postharvest strawberry fruit. *Food Chemistry, 285*, 163–170.
Li, Y., Hu, Z., Huo, R., & Cui, Z. (2023). Preparation of an indicator film based on pectin, sodium alginate, and xanthan gum containing blueberry anthocyanin extract and its application in blueberry freshness monitoring. *Heliyon, 9*(3).
Liu, R., Wang, X., Yang, L., Wang, Y., & Gao, X. (2023). Coordinated encapsulation by β-cyclodextrin and chitosan derivatives improves the stability of anthocyanins. *International Journal of Biological Macromolecules, 242*, Article 125060.
Liu, Y., Lin, J., Cheng, T., Liu, Y., & Han, F. (2022). Methylation, hydroxylation, glycosylation and acylation affect the transport of wine anthocyanins in Caco-2 cells. *Foods, 11*(23), 3793.
Ma, Z., Zhao, J., Zou, Y., & Mao, X. (2024). The enhanced affinity of moderately hydrolyzed whey protein to EGCG promotes the isoelectric separation and unlocks the protective effects on polyphenols. *Food Chemistry, 450*, Article 138833.
Mansour, M., Salah, M., & Xu, X. (2020). Effect of microencapsulation using soy protein isolate and gum arabic as wall material on red raspberry anthocyanin stability, characterization, and simulated gastrointestinal conditions. *Ultrasonics Sonochemistry, 63*, Article 104927.
Mao, Y., & McClements, D. (2012). Influence of electrostatic heteroaggregation of lipid droplets on their stability and digestibility under simulated gastrointestinal conditions[J]. *Food & Function, 3*(10), 1025–1034.
Mu, Y., Fu, Y., Li, J., Yu, X., Li, Y., Wang, Y., … Chen, X. (2019). Multifunctional quercetin conjugated chitosan nano-micelles with P-gp inhibition and permeation enhancement of anticancer drug. *Carbohydrate Polymers, 203*, 10–18.
Mundlia, J., Ahuja, M., & Kumar, P. (2021). Enhanced biological activity of polyphenols on conjugation with gellan gum. *International Journal of Polymeric Materials and Polymeric Biomaterials, 70*(10), 712–729.
Tao, X., Shi, H., Cao, A., & Cai, L. (2022). Influence of polyphenol-metal ion-coated ovalbumin/sodium alginate composite nanoparticles on the encapsulation of kaempferol/tannin acid. *International Journal of Biological Macromolecules, 209*, 1288–1297.
Veberic, R., Slatnar, A., Bizjak, J., Stampar, F., & Mikulic-Petkovsek, M. (2015). Anthocyanin composition of different wild and cultivated berry species. *LWT-Food Science and Technology, 60*, 509–517.
Wang, H., Wang, C., Fan, W., Yang, J., Appelhagen, I., Wu, Y., & Zhang, P. (2018). A novel glycosyltransferase catalyses the transfer of glucose to glucosylated anthocyanins in purple sweet potato. *Journal of Experimental Botany, 69*(22), 5444–5459.
Wang, S., Ye, X., Sun, Y., Liang, J., Yue, P., & Gao, X. (2021). Nanocomplexes derived from chitosan and whey protein isolate enhance the thermal stability and slow the release of anthocyanins in simulated digestion and prepared instant coffee. *Food Chemistry, 336*, Article 127707.
Wu, T., Cheng, J., Zhang, J., Zhao, H., Sui, W., Zhu, Q., … Zhang, M. (2022). Hypoglycemic activity of self-assembled Gellan gum-soybean isolate composite hydrogel-embedded active substance-Saponin. *Foods, 11*(22), 3729.
Xu, X. J., Fang, S., Li, Y. H., Zhang, F., Shao, Z. P., Zeng, Y. T., … Meng, Y. C. (2019). Effects of low acyl and high acyl gellan gum on the thermal stability of purple sweet potato anthocyanins in the presence of ascorbic acid. *Food Hydrocolloids, 86*, 116–123.
Xue, B., Wang, Y., Tian, J., Zhang, W., Zang, Z., Cui, H., … Liu, R. H. (2022). Effects of chitooligosaccharide-functionalized graphene oxide on stability, simulated digestion, and antioxidant activity of blueberry anthocyanins. *Food Chemistry, 368*, Article 130684.
Zang, Z., Chou, S., Geng, L., Si, X., Ding, Y., Lang, Y., … Tian, J. (2021). Interactions of blueberry anthocyanins with whey protein isolate and bovine serum protein: Color stability, antioxidant activity, in vitro simulation, and protein functionality. *Lwt, 152*, Article 112269.
Zang, Z., Chou, S., Si, X., Cui, H., Tan, H., Ding, Y., & Tian, J. (2022). Effect of bovine serum albumin on the stability and antioxidant activity of blueberry anthocyanins during processing and in vitro simulated digestion. *Food Chemistry, 373*, Article 131496.
Zhu, D., Damodaran, S., & Lucey, J. A. (2008). Formation of whey protein isolate (WPI)–dextran conjugates in aqueous solutions. *Journal of Agricultural and Food Chemistry, 56*(16), 7113–7118.